TISSUE ENGINEERING: Part A
Volume 26, Numbers 9 and 10, 2020

DOI: 10.1089/ten.tea.2019.0227

termis
Tissue Engineering
& Regenerative Medicine
International Society

ORIGINAL ARTICLE

Human Stem Cell-derived Aggregates of Forebrain Astroglia Respond to Amyloid Beta Oligomers

Kyle Griffin, BS,[1] Julie Bejoy, PhD,[1,*] Liqing Song, PhD,[1,†] Thien Hua, MS,[2] Mark Marzano, MS,[1] Richard Jeske, BS,[1] Qing-Xiang Amy Sang, PhD,[2,3] and Yan Li, PhD[1,3]

Astrocytes are vital components in neuronal circuitry and there is increasing evidence linking the dysfunction of these cells to a number of central nervous system diseases. Studying the role of these cells in human brain function in the past has been difficult due to limited access to the human brain. In this study, human induced pluripotent stem cells were differentiated into astrospheres using a hybrid plating method, with or without dual SMAD inhibition. The derived cells were assessed for astrocytic markers, brain regional identity, phagocytosis, calcium-transient signaling, reactive oxygen species production, and immune response. Neural degeneration was modeled by stimulation with amyloid-β (Aβ) 42 oligomers. Finally, co-culture was performed for the derived astrospheres with isogenic neurospheres. Results indicate that the derived astroglial cells express astrocyte markers with forebrain dorsal cortical identity, secrete extracellular matrix, and are capable of phagocytosing iron oxide particles and responding to Aβ42 stimulation (higher oxidative stress, higher TNF-α, and IL-6 expression). RNA-sequencing results reveal the distinct transcriptome of the derived cells responding to Aβ42 stimulation for astrocyte markers, chemokines, and brain regional identity. Co-culture experiments show the synaptic activities of neurons and the enhanced neural protection ability of the astroglial cells. This study provides knowledge about the roles of brain astroglial cells, heterotypic cell-cell interactions, and the formation of engineered neuronal synapses *in vitro*. The implications lie in neurological disease modeling, drug screening, and studying progression of neural degeneration and the role of stem cell microenvironment.

Keywords: human pluripotent stem cells, astrocytes, spheroids, inflammation, neural degeneration

Impact Statement

Human pluripotent stem cell-derived astrocytes are a powerful tool for disease modeling and drug screening. However, the properties regarding brain regional identity and the immune response to neural degeneration stimulus have not been well characterized. Results of this study indicate that the derived astroglial cells express astrocyte markers with forebrain dorsal cortical identity, secrete extracellular matrix (ECM), and are capable of phagocytosing iron oxide particles and responding to amyloid-β oligomers, showing the distinct transcriptome in astrocyte markers, chemokines, and brain regional identity. This study provides knowledge about the roles of brain astroglial cells, heterotypic cell-cell interactions, and engineering neural tissues *in vitro*.

Introduction

The most abundant cells in the human brain are astroglial cells, which account for 20–40% of total brain cells.[1] Astrocyte to neuron ratio is increased in humans compared to rodents and varies between human brain regions. For example, in the cerebral cortex, astrocytes outnumber neurons (3:1–5:1), while in the cerebellum, neurons greatly outnumber astrocytes. Astrocytes serve as the energy supply to neurons and help to form and maintain synapses.[2,3] They

[1]Department of Chemical and Biomedical Engineering, FAMU-FSU College of Engineering, Florida State University, Tallahassee, Florida, USA.
[2]Department of Chemistry and Biochemistry, Florida State University, Tallahassee, Florida, USA.
[3]Institute of Molecular Biophysics, Florida State University, Tallahassee, Florida, USA.
**Current address:* College of Medicine, Vanderbilt University, Nashville, Tennessee, USA.
[†]*Current address:* Department of Chemical Engineering, Carnegie Mellon University, Pittsburgh, Pennsylvania, USA.

are also the essential components of blood–brain barrier (BBB) in the brain.[4–6] Human astrocytes are 20 times larger and integrate 20 times more synapse than the rodent cells. They also propagate Ca^{2+} waves more quickly than rodent cells.[7] In addition, astrocytes secrete neurotrophic factors and provide matrix support for proper neuron function.[8] They strongly respond to ATP and mediate microglial response to inflammatory stimuli (such as amyloid-β [Aβ]).[9] Several questions emerged recently about the roles of astrocytes in human brain function. For example, how astrocytes contribute to the formation and functions of synapses and circuits.[10] Using human induced pluripotent stem cells (hiPSCs) as a tool may help to answer these questions.

Generating astrocytes from hiPSCs has been reported by several studies,[11,12] but is ultimately hindered by insufficient knowledge of astrocyte specification during neural tissue development and by the lack of specific astrocyte markers. A few studies have reported the generation of inflammation-responsive astrocytes.[9,13] As one example, starting from hiPSC-derived neural progenitor cells, 11 methods were screened for efficient astrocyte generation in 30 days[14] based on astrocyte markers GFAP, S100B, AQU4, vimentin, and APOE. Transcriptome analysis showed similar signature compared to human fetal astrocytes. The derived astrocytes were able to secrete IL-1β, IL-4, 6, 8, and 10 and TNF-α stimulated by Aβ42 and lipopolysaccharides (LPS). Since astrocyte differentiation from hiPSCs usually has long procedure (>40 days) and inefficient differentiation yield, overexpression of SOX9 and NFIB in hPSCs can be implemented to rapidly generate astrocytes (>88% GFAP, S100B, and vimentin) in 7 days.[15,16] However, hiPSC-derived astrocytes were also reported to be at immature fetal-like status based on RNA-sequencing data and less functional than neonatal mouse cortical astrocytes.[17] In addition, astrocytes have many subtypes depending on their locations, molecular signature, and physiological functions, which have not been fully understood.[10] Such heterogeneity was suggested to come from regional patterning of the neural progenitors.[18] Novel culture strategy such as 3D culture may help to mature hiPSC-derived astrocytes.[19]

Astrocytes have been derived from 3D cerebral organoids through dissociation, enzymatic digestion, and replating on laminin surface.[11] In 3D cortical spheroid formation, nonreactive astrocytes were co-differentiated from hiPSCs along with deep and superficial cortical layers.[20] 3D astrospheres were also co-cultured with organoid spheres of hiPSC-derived neural progenitors.[21] Enhanced astrocytic complexity (''gray-matter'' like morphology) was observed in 3D organotypic-like co-culture environment. The 3D culture-derived astrocytes were found to transit from a predominantly fetal to an increasingly mature astrocyte state,[19] indicated by alterations in phagocytic capacity and effects on neuronal calcium signaling.

Human iPSC-derived astrocytes are a powerful tool for disease modeling. PSEN1 ΔE9 mutant hiPSCs can differentiate into astrocytes expressing GFAP and S100B, astrocyte-specific glutamate transporters SLC1A2 and SLC1A3, and water channel AQP4.[2] γ-Secretase inhibitor DAPT treatment decreased Aβ40 and Aβ42 production in iPSC astrocytes from both Alzheimer's disease (AD) patients and healthy control. PSEN1 astrocytes secreted significantly higher levels of IL-2, IL-6, and IL-10 and GM-CSF stimulated by IL-1β and TNF-α than control astrocytes. Human iPSCs with APOE ε4/ε4 mutants were able to differentiate into astrocytes expressing GFAP, S100B, AQP4, and vimentin, and were secreting APOE. iPSC-derived astrocytes promoted neuronal survival depending on APOE genotype (APOE3 genotype better supported neural survival than APOE4 genotype, 46% vs. 31%).[22] Using CRISPR-Cas9 and hiPSCs to generate APOE4-iPSCs, the effects of APOE4 on different brain cell types (e.g., neurons, astrocytes, and microglia) were examined.[23] APOE4 astrocytes can uptake oligomeric Aβ42 and contribute to Aβ clearance.

To evaluate heterotypic cell-cell interactions of astrocytes and neurons, this study derived and characterized astrocyte spheroids (e.g., RNA-sequencing, calcium signaling, reactive oxygen species (ROS), and neural inflammation upon Aβ42 oligomer stimulation) and then co-cultured them with isogenic cortical spheroids. It is hypothesized that the presence of astrocytes in cortical spheroids would promote tissue homeostasis and neural protective ability. This study directly addressed several aspects of healthy iPSC-derived astrocyte behavior and immune response under homeostatic and AD-associated conditions.

Materials and Methods

Undifferentiated hiPSC culture

Human iPSK3 cells were derived from human foreskin fibroblasts transfected with plasmid DNA, encoding reprogramming factors OCT4, NANOG, SOX2, and LIN28 (kindly provided by Dr. Stephen Duncan, Medical College of Wisconsin).[24,25] Human iPSK3 cells were maintained in mTeSR serum-free medium (StemCell Technologies, Inc., Vancouver, Canada) on growth factor-reduced Geltrex or Matrigel-coated surface (Life Technologies).[26] The cells were passaged by Accutase every 7 days and seeded at 1×10^6 cells per well of a six-well plate in the presence of 10 μM Y27632 (Sigma) for the first 24 h.[26–28] The undifferentiated iPSK3 cells expressed Oct-4, the pluripotency marker, and F-actin cytoskeleton (Supplementary Fig. S1).

Human Ep-iPSC cells were obtained commercially from ThermoFisher (Cat No. A18945). The Gibco Human Episomal iPSC Line was derived from $CD34^+$ cord blood using a three-plasmid, seven-factor [SOKMNLT; SOX2, OCT4 (POU5F1), KLF4, MYC, NANOG, LIN28, and SV40L T antigen] EBNA-based episomal system. This iPSC line is considered to be zero footprint as there was no integration into the genome from the reprogramming event and is free of all reprogramming genes. Ep-iPSC cells were maintained in StemFlex™ Medium (ThermoFisher) on growth factor-reduced Geltrex or Matrigel-coated surface. The cells were passaged by Versene (ThermoFisher) every 3–4 days and seeded at 1:8–1:12 ratio onto the new surface.

Astrosphere differentiation

Human iPSCs were seeded into Ultra-Low Attachment (ULA) 24-well plates (Corning Incorporated, Corning, NY) at 3×10^5 cells/well in 1 mL of differentiation medium composed of Dulbecco's modified Eagle's medium/Nutrient Mixture F-12 (DMEM/F-12) plus 2% B27 serum-free supplement (Life Technologies). Y27632 (10 μM) was added during the seeding and removed after 24 h. On day 1, the cells formed embryoid bodies (EBs) and were treated with dual

SMAD signaling inhibitors 10 μM SB431542 (Sigma) and 100 nM LDN193189 (Sigma) (referred as LDN/SB$^+$ group) or without any factors (referred as LDN/SB$^-$ group).[27] After 8 days, the cells were treated with fibroblast growth factor (FGF)-2 (10–50 ng/mL; Life Technologies), epidermal growth factors (EGF) (10–50 ng/mL; Peprotech), and 5 μg/mL heparin until day 14. On day 15, the spheroids were fed with astrocyte induction medium: DMEM/F-12 plus 2% B27, retinoic acid (RA; Sigma) at 0.5 μM, and heparin at 2 μg/mL for another 12 days. On day 27–36, astrospheres were dissociated with Accutase and replated onto Geltrex-coated plates at 2.5×10^4 cells/cm^2 in astrocyte medium: DMEM/F-12 plus 2% B27 and heparin at 2 μg/mL (no RA). The media were changed every other day for at least another 2 weeks (40–60 days in total) before characterizations.[5]

For cortical neural differentiation, human iPSK3 cells were seeded into ULA 24-well plates at 3×10^5 cells/well in 1 mL of differentiation medium composed of DMEM/F-12 plus 2% B27 serum-free supplement plus Y27632 (10 μM) for 24 h. On day 1, the cells formed EBs and were treated with 10 μM SB431542 and 100 nM LDN193189.[27,29,30] After 8 days, the cells were treated with FGF-2 (10 ng/mL) and RA (5 μM) until day 16. On day 17, the spheroids were replated to Geltrex-coated plates and used for characterizations or co-culture.

Treatments with Aβ(1–42) oligomers and LIVE/DEAD assay

To prepare oligomers of the Aβ42 peptide, biotinylated Aβ42 (Bachem) was fully dissolved at 0.5 mg/mL in hexafluor-2-propanole (HFIP; Sigma).[29,31] Ten microliters of HFIP Aβ(1–42) solution was dispensed into a siliconized Snap-Cap microtube, put in a desiccator to completely evaporate HFIP, and thereafter stored at −80°C. Oligomer solutions were prepared freshly for each experiment. The stock was dissolved in 10 μL of DMSO (to 105 μM) and incubated for 3 h at room temperature. Oligomers of Aβ42 (at 1 μM) were added to the day 40 astrocyte cultures (in 96-wp). LIVE/DEAD assay and ROS assay were performed for Aβ42 oligomer-treated cultures. The cells were evaluated for viability using Live/Dead® staining kit (Molecular Probes). After 72 h, the cells were incubated in DMEM-F12 containing 1 μM calcein-AM (green) and 2 μM ethidium homodimer I (red) for 30 min. The samples were imaged under a fluorescent microscope (Olympus IX70, Melville, NY) or quantified by flow cytometry. Using ImageJ software, the viability was calculated as the percentage of green intensity over total intensity (including both green cells and red cells).

Immunocytochemistry

Briefly, the samples were fixed with 4% paraformaldehyde (PFA) and permeabilized with 0.2–0.5% Triton X-100. The samples were then blocked for 30 min and incubated with various mouse or rabbit primary antibodies (Supplementary Table S1) for 4 h. After washing, the cells were incubated with the corresponding secondary antibody: Alexa Fluor® 488 goat anti-Mouse IgG_1, Alexa Fluor 594 goat anti-Rabbit IgG, or 594 donkey anti-goat IgG (Life Technologies), for 1 h. The samples were counterstained with Hoechst 33342 and visualized using a fluorescent microscope (Olympus IX70).[29,32]

Flow cytometry

To quantify the levels of various marker expressions, the cells were harvested by trypsinization and analyzed by flow cytometry.[33] Briefly, 1×10^6 cells per sample were fixed with 4% PFA and washed with staining buffer (2% fetal bovine serum in phosphate-buffered saline). The cells were permeabilized with 100% cold methanol, blocked, and then incubated with various primary antibodies (Supplementary Table S1) followed by the corresponding secondary antibody Alexa Fluor 488 goat anti-Mouse IgG_1 or Alexa Fluor 594 Goat Anti-rabbit or Donkey Anti-Goat IgG. The cells were acquired with BD FACSCanto™ II flow cytometer (Becton Dickinson) and analyzed against isotype controls using FlowJo software.

Phagocytosis assay

The day 40 derived cells in 24-well plate were incubated with medium containing $0.25–1.0 \times 10^8$ fluorescent (0.86 μm, flash red, 660/690 nm) micron-sized particles of iron oxide (MPIO)/mL (Part number ME03F/9772; Bangs Laboratories, Fishers, IN) corresponding to the concentration at 2.5–10 μg Fe/mL.[34,35] The attached cells that were not labeled with MPIO served as control. After a 24-h incubation, the cultures labeled with MPIO were extensively washed (10 times) with phosphate-buffered saline. The cultures were then harvested for flow cytometry to quantify the cells with MPIO.

Enzyme-linked immunosorbent assay

To quantify the growth factors secreted by stimulated or unstimulated astrocytes, culture supernatants were collected on day 3 after the stimulation. Concentrations of vascular endothelial growth factor A (VEGF-A) was measured by enzyme-linked immunosorbent assay (ELISA) according to the manufacturers' instructions (Life Technologies). Briefly, the samples were added into 96-wps and incubated with primary/secondary antibody solution conjugated with horseradish peroxidase for 2–3 h. After washing, 3,3′,5,5′-tetramethylbenzidine substrate solution was added and the mixture was incubated for 30 min. The absorbance units were measured using a microplate reader (Bio-Rad, Richmond, CA).

ROS assay

ROS detection was performed using Image-iT™ Live Green Reactive Oxygen Species Detection kit (Molecular probes).[36,37] Briefly, the cells were washed in Hank's Balanced Salt Solution (HBSS), and incubated in a solution of 25 μM carboxy-H_2DCFDA for 30 min at 37°C. The samples (with or without Aβ42 oligomer stimulation) were then washed and analyzed under fluorescence microscope or by flow cytometry. As positive control, the cells were incubated in a 100 μM tert-butyl hydroperoxide (TBHP) solution, before staining with carboxy-H_2DCFDA.

Intracellular Ca^{2+} signaling assay

For calcium signaling, the samples were replated on 1% Geltrex-coated 96-well plate and grown overnight. The growth medium was removed in each well and 100 μL of 1 × Fluo-4 dye (Life Technologies) in assay buffer containing 1 × HBSS and 20 mM HEPES (with 2.5 mM probenecid)

was added into the wells and incubated at 37°C for 30 min. The incubation was switched to room temperature for an additional 30 min. Baseline Ca^{2+} signals (I_{494}/I_{516}) were measured for more than 100 s, and then the calcium dye medium was replaced with 100 μL of 10 μM adenosine 5′-diphosphate (ADP; Sigma) solution in assay buffer (without probenecid). Ca^{2+} recordings were read on a fluorescent plate reader (FLX800; Bioinstrument, Inc., Winooski, VT) using instrument settings appropriate for excitation at 494 nm and emission at 516 nm.

Reverse transcription-polymerase chain reaction analysis

Total RNA was isolated from different cell samples using the RNeasy Mini Kit (Qiagen, Valencia, CA) according to the manufacturer's protocol, followed by the treatment of DNA-Free RNA Kit (Zymo, Irvine, CA).[28] Reverse transcription was carried out using 2 μg of total RNA, anchored oligo-dT primers (Operon, Huntsville, AL), and Superscript III (Invitrogen, Carlsbad, CA) (according to the protocol of the manufacturer). Primers specific for target genes (Supplementary Table S2) were designed using the software Oligo Explorer 1.2 (Genelink, Hawthorne, NY). The gene β-actin was used as an endogenous control for normalization of expression levels. Real-time reverse transcription-polymerase chain reaction (RT-PCRs) was performed on an ABI7500 instrument (Applied Biosystems, Foster City, CA), using SYBR1 Green PCR Master Mix (Applied Biosystems). The amplification reactions were performed as follows: 2 min at 50°C, 10 min at 95°C, and 40 cycles of 95°C for 15 s and 55°C for 30 s, and 68°C for 30 s. Fold variation in gene expression was quantified by means of the comparative Ct method: $2^{-(\Delta C_{t\ \text{treatment}} - \Delta C_{t\ \text{control}})}$, which is based on the comparison of expression of the target gene (normalized to the endogenous control β-actin) between the compared samples.

RNA extraction and RNA-Seq cDNA library preparation

RNA was extracted from the LDN/SB$^+$ condition-derived astrocytes (minus group) or those treated with Aβ42 oligomers (plus group) on day 42 using the miRNeasy mini kit (Qiagen). mRNA was isolated from the total RNA using an NEBNext Poly(A) mRNA Magnetic Isolation Module (New England Biolabs). cDNA libraries were generated from the isolated

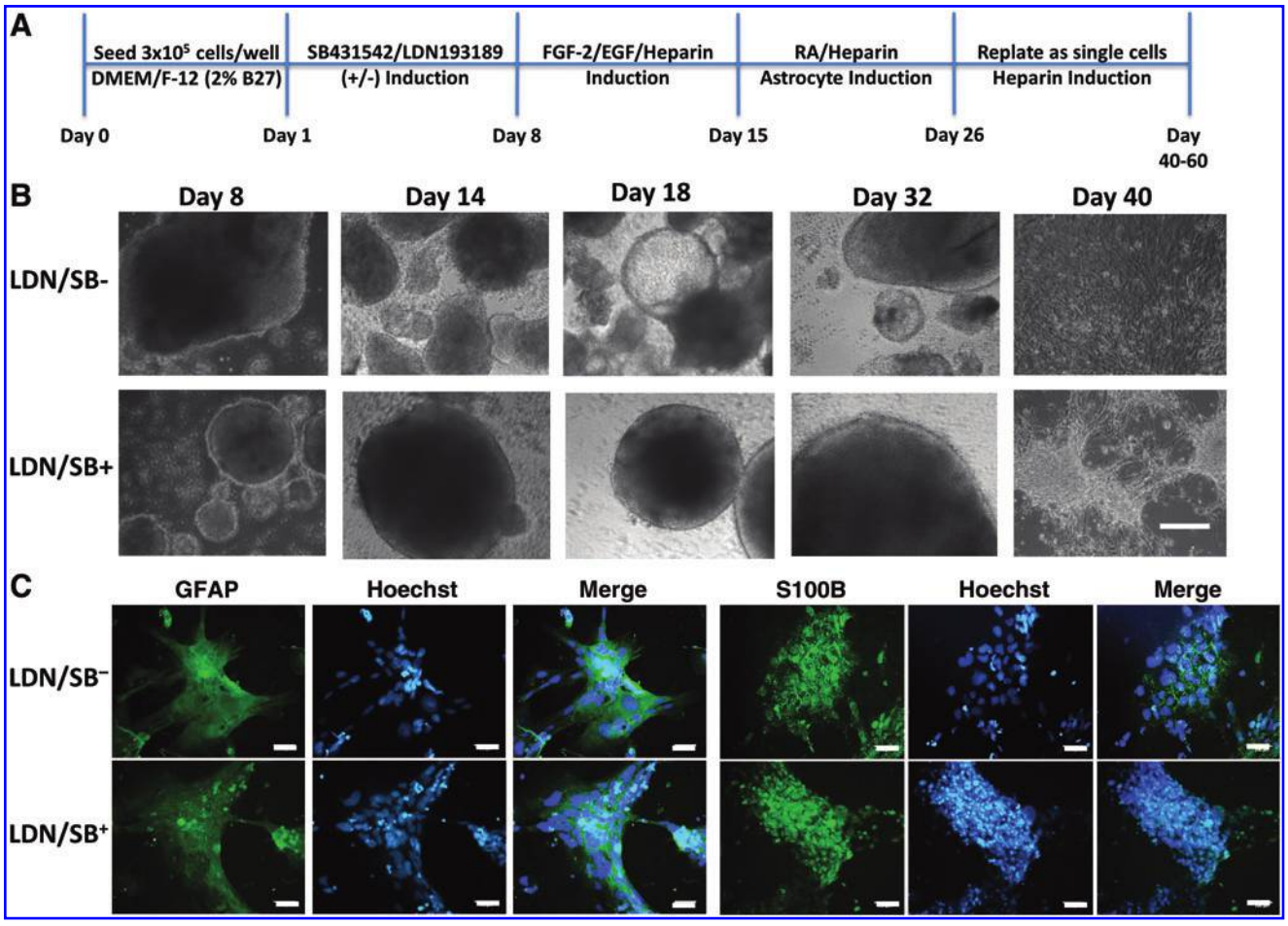

FIG. 1. Generation of asteroids from hiPSCs. **(A)** Outline of differentiation stages for generating asteroids. Half of the samples receive dual SMAD inhibition for the first week, while the other half do not. Asteroids are dissociated and replated as single cells on day 26–33. **(B)** Phase-contrast images of morphology over the time for asteroids of both LDN/SB$^-$ and LDN/SB$^+$ conditions. Scale bar: 200 μm. **(C)** Immunostaining of GFAP and S100B of astrocytic cultures. Scale bar: 100 μm. hiPSCs, human induced pluripotent stem cells. Color images are available online.

mRNA using an NEBNext Ultra RNA library prep kit for Illumina (New England Biolabs), and a unique 6 nucleotide index primer (NEBNext multiplex oligos for Illumina) was incorporated into each sample. The library construction was done according to the NEB manuals, modified for use with a Beckman Biomek 4000 at the Florida State University Biological Sciences core laboratory. The unique index (barcode) was added to each library to multiplex the libraries. The multiplexed sample was quantified with quantitative PCR (Kapa Biosystems) specific for Illumina sequencing primers and the average fragment size was determined with a Bioanalyzer high sensitivity DNA chip (Agilent Technologies). The pooled sample was sequenced, with single-end, 100 base reads on an Illumina NovaSeq 6000 located in the Translational Science Laboratory at the College of Medicine, Florida State University. The pooled data were demultiplexed into individual sample data and adapter primer sequences were removed.[38]

RNA-Seq data analysis

Initial quality control analysis of each sequenced library was performed using fastQC software. The sequencing reads were further analyzed using RNA-Seq Alignment version 1.1.1 (Illumina BaseSpace application). The reads were aligned with Star 2.6.1a[39] to the human genome (genome release GRCh38) using default parameters and counts for each gene were generated. These normalized values account for differences in sequencing depth and the length of the gene. DESeq2 was used to determine statistically significant differentially expressed genes (DEGs) (a false discovery rate, FDR, of <0.05 was used). Around 14,926 genes were considered to be expressed in this study by the DESeq2 software due to low counts.[40] The genes that were upregulated and downregulated in the minus culture versus the plus group were further assessed for GO, KEGG pathway, and

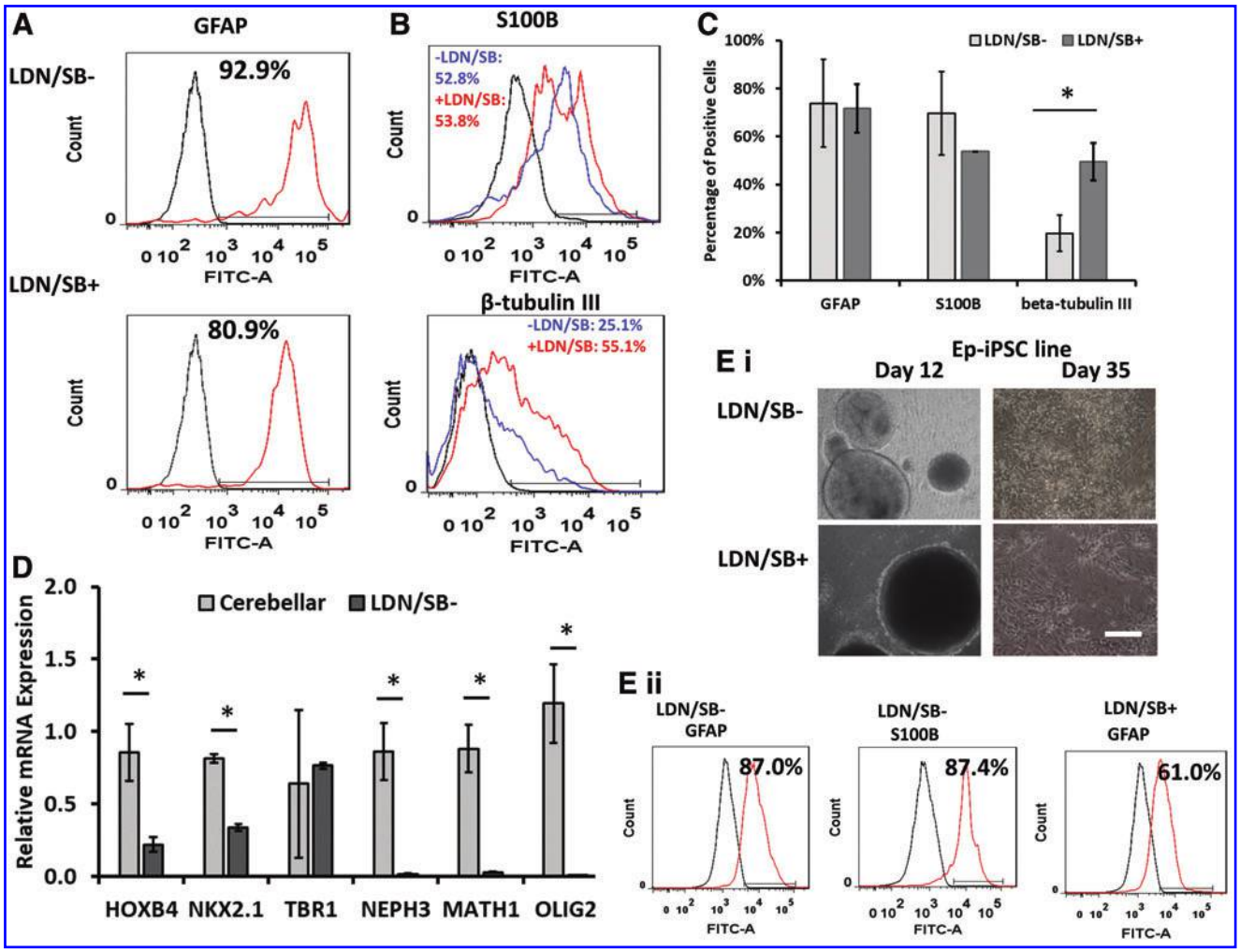

FIG. 2. Characterization of hiPSC-derived asteroids by flow cytometry and RT-PCR. The differentiation was performed using iPSK3 line for **(A–D)**. **(A)** Representative expression of GFAP determined by flow cytometry. **(B)** Representative expression of S100B and β-tubulin III quantified by flow cytometry. *Black line*: negative control; *red line* or *blue line*: marker of interest. **(C)** Average marker expression determined by flow cytometry ($n=3$). **(D)** Gene expression of brain regional markers by RT-PCR analysis (LDN/SB$^-$ group) ($n=3$). HOXB4: a hindbrain marker; hindbrain cerebellar markers: NEPH3, MATH1, and OLIG2. Nkx2.1: a ventral forebrain cortical marker; TBR1: a dorsal forebrain cortical marker. *indicates $p<0.05$. **(E)** The differentiation was performed using Ep-iPSC line. (i) Phase-contrast images of morphology over the time for asteroids of both LDN/SB$^-$ and LDN/SB$^+$ conditions. Scale bar: 200 μm. (ii) Expression of GFAP and S100B quantified by flow cytometry. *Black line*: negative control; *red line* or *blue line*: marker of interest. RT-PCR, reverse transcription-polymerase chain reaction. Color images are available online.

phenotype pathway analysis using Webgestalt.[41,42] The set of genes considered expressed in our dataset was used as the reference set to obtain significantly enriched pathways. Significant enrichment was determined in Webgestalt using the hypergeometric test and the Benjamini–Hochberg FDR method[43] for multiple testing adjustment.

Co-culture of cortical spheroids with the derived astrospheres

Cortical spheroid differentiation was performed as previously described.[30,31,44,45] For co-culture, the day 40 cortical spheroids were replated onto the day 53 astrocyte layer, which was treated with 1 μM Aβ42 oligomers. The ratio of neurons to astrocytes was estimated to be 1:1. LIVE/DEAD assay was performed 7 days after the co-culture. The cortical spheroids only treated with Aβ42 oligomers served as control. Another co-culture method was also performed. The dissociated day 40 small astrospheres in suspension were labeled with CellTracker Green (2.5 μM; Life Technologies) for 30 min. The labeled astrospheres were added to the wells containing day 40 cortical spheroids (1:1 ratio of neurons to astrocytes). The ability of small astrospheres to fuse with cortical spheroids was monitored using a fluorescent microscope.[46] The co-cultured spheroids were replated onto Geltrex-coated surface for 3 days. Immunostaining for synaptic markers was performed with cortical spheroid monoculture as control.

Statistical analysis

The representative experiments are presented and the results are expressed as (mean ± standard deviation). To assess the statistical significance, one-way ANOVA followed by Fisher's LSD *post hoc* tests were performed. A p-value <0.05 was considered statistically significant.

Results

Differentiation and characterizations of iPSK3-derived asteroids

Upon passage, iPSK3 cells were cultured in suspension and subjected to either dual SMAD inhibition with LDN193189 and SB431542 (hereinafter called "LDN/SB^{+}") or without the treatment (LDN/SB^{-}) for the first 7 days *in vitro* (Fig. 1A). After the first day, EBs were formed for both conditions (Fig. 1B). LDN/SB^{-}-derived EBs seemed denser than LDN/SB^{+}-derived EBs and had a dark flake-like appearance, whereas the latter were lighter in color and sphere like. All cultures were treated with EGF/FGF-2/heparin until day 14 for neural progenitor expansion; then the factors were switched to RA/heparin until day 26 for astrosphere induction. After dissociating and replating, only heparin was used for further maturation until day 40–60. Immunostaining showed GFAP expression mainly localized in the cytoplasm (Fig. 1C). S100B was localized in the cytoplasm and nucleus. Additional astrocyte marker vimentin was also expressed in the derived cells

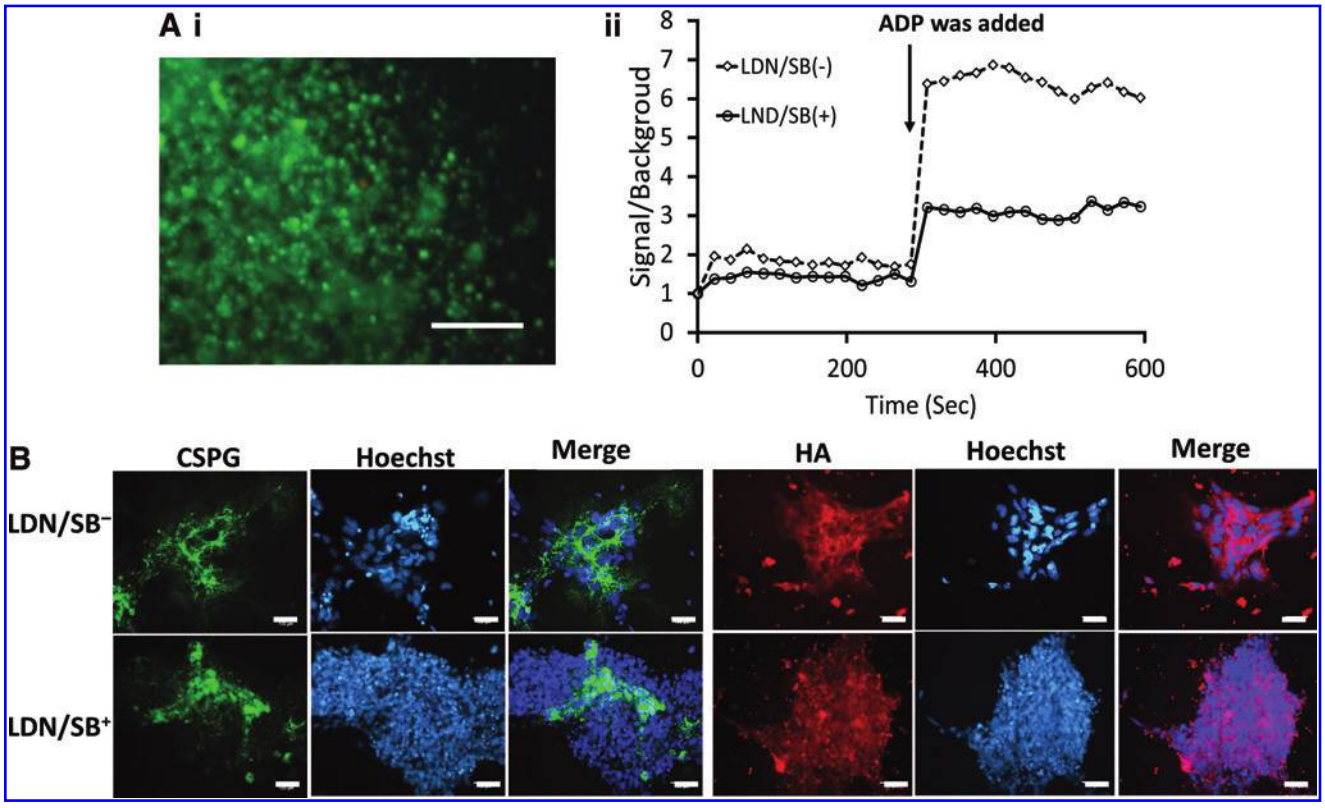

FIG. 3. Calcium activity and extracellular matrix characterization of iPSK3-derived asteroids. **(A)** (i) Fluorescent image that shows Ca^{2+} signaling (day 45); (ii) fluorescence reading of ADP treatment-induced Ca^{2+} change from baseline. **(B)** Immunostaining of CSPG and HA on the replated asteroids (day 50). *Blue*: Hoechst 33342 for nuclei. Scale bar: 100 μm. ADP, adenosine 5′-diphosphate; CSPG, chondroitin sulfate proteoglycans; HA, hyaluronic acid. Color images are available online.

(Supplementary Fig. S2A). From flow cytometry quantification (Fig. 2–C), a large population of GFAP$^+$ cells (92.9% and 80.9%) was observed, and S100B expression was similar for the two conditions (52.8–53.8%). Dual SMAD inhibition (LDN/SB$^+$) resulted in more β-tubulin III$^+$ cells when comparing to LDN/SB$^-$ group (55.1% vs. 25.1%), suggesting that LDN/SB treatment enriches neuronal population (Fig. 2B, C).

To determine the brain regional identity of the derived cells, GFAP was co-stained with regional identity markers: FOXG1 (cortical dorsal identity), Nkx2.1 (cortical ventral identity), and HOXB4 (hindbrain identity). A majority of the cells expressed FOXG1 with some Nkx2.1 expression, showing the astrocytes with cortical dorsal identity (Supplementary Fig. S2B, C). The presence of some hindbrain (HOXB4$^+$) astrocytes was observed. The mRNA expression of brain regional identity markers was quantified by RT-PCR for LDN/SB$^-$ group (the yield of LDN/SB$^+$ group was too low, and the cells were unable to be analyzed) (Fig. 2D). The isogenic hindbrain cerebellar spheroids were used as the control (Supplementary Data).[47] The expression levels of hindbrain marker HOXB4, hindbrain cerebellar markers NEPH3, MATH1, and OLIG2,[47] and the ventral forebrain cortical marker Nkx2.1 were significantly lower for the astrospheres. However, the expression of dorsal forebrain cortical marker TBR1 was comparable for the two groups. These results confirm the dorsal cortical identity of the astrospheres.

The astroglial differentiation was also performed using Ep-iPSC line (Fig. 2E). A large population of GFAP$^+$ cells (61.0% and 87.0%) was observed, and S100B expression was high (87.4%) for the LDN/SB$^-$ group. Since LDN/SB$^+$ condition resulted in lower yield, S100B flow cytometry was not performed due to an insufficient number of cells.

Astrocytes use Ca^{2+} signaling for intercellular communication[10,48]; thus, exhibition of the calcium signaling is an important indicator of astrocyte function. Fluo-4 dye was added to the cells of LDN/SB$^-$ and LDN/SB$^+$ groups (Fig. 3A). Upon ADP stimulation, the cells showed significant Ca^{2+} signals (I_{494}/I_{516}). ECM secretion, including chondroitin sulfate proteoglycan (CSPG) and hyaluronic acid (HA), was also visible by the derived cells (Fig. 3B). Phagocytosis ability was shown by MPIO internalization as quantified by flow cytometry (50.1%) (Fig. 4). The co-staining with GFAP indicates that the GFAP$^+$ cells, but few GFAP$^-$ cells (2.5–4.0%), phagocytosed MPIO. The lower MPIO$^+$ cells (24.4–28.3%) in co-stained cells may be due to the permeabilization of GFAP staining.

Response to Aβ42 oligomers stimulation

As previously mentioned, accumulation of Aβ42 oligomers in the extracellular space is a hallmark of AD.[49] In this study, the effects of Aβ42 oligomers were assessed in regard to viability, ROS production, VEGF-A secretion, neural

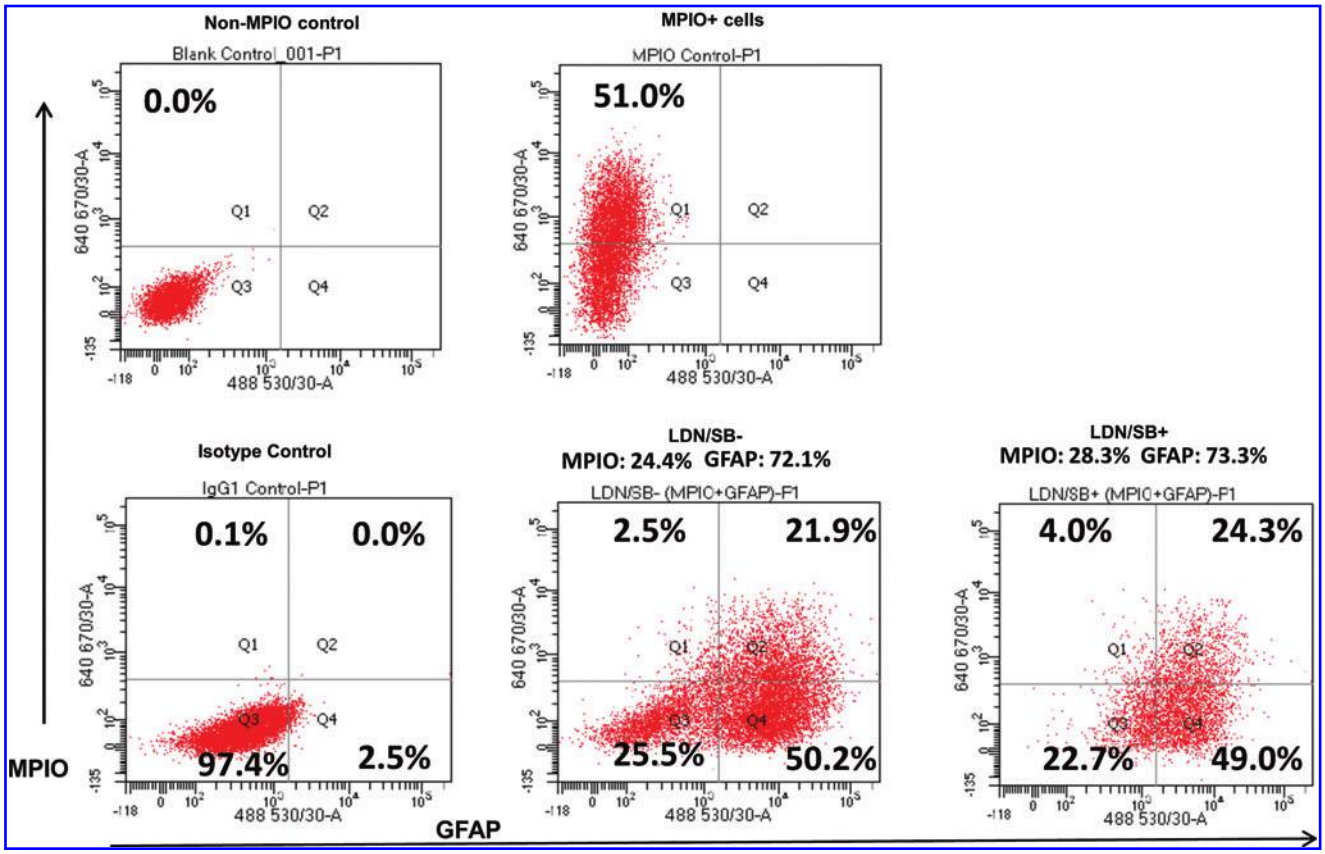

FIG. 4. Phagocytosis ability of the replated iPSK3-derived asteroids (day 40). The replated cells were exposed to MPIO at the concentration of 5 μg Fe/mL for 24 h. The cells were then harvested, fixed, and stained for the expression of GFAP. The MPIO$^+$ cells (Alexa 647) and GFAP$^+$ cells (Alexa 488) were quantified by two-color flow cytometry. MPIO, micron-sized particles of iron oxide. Color images are available online.

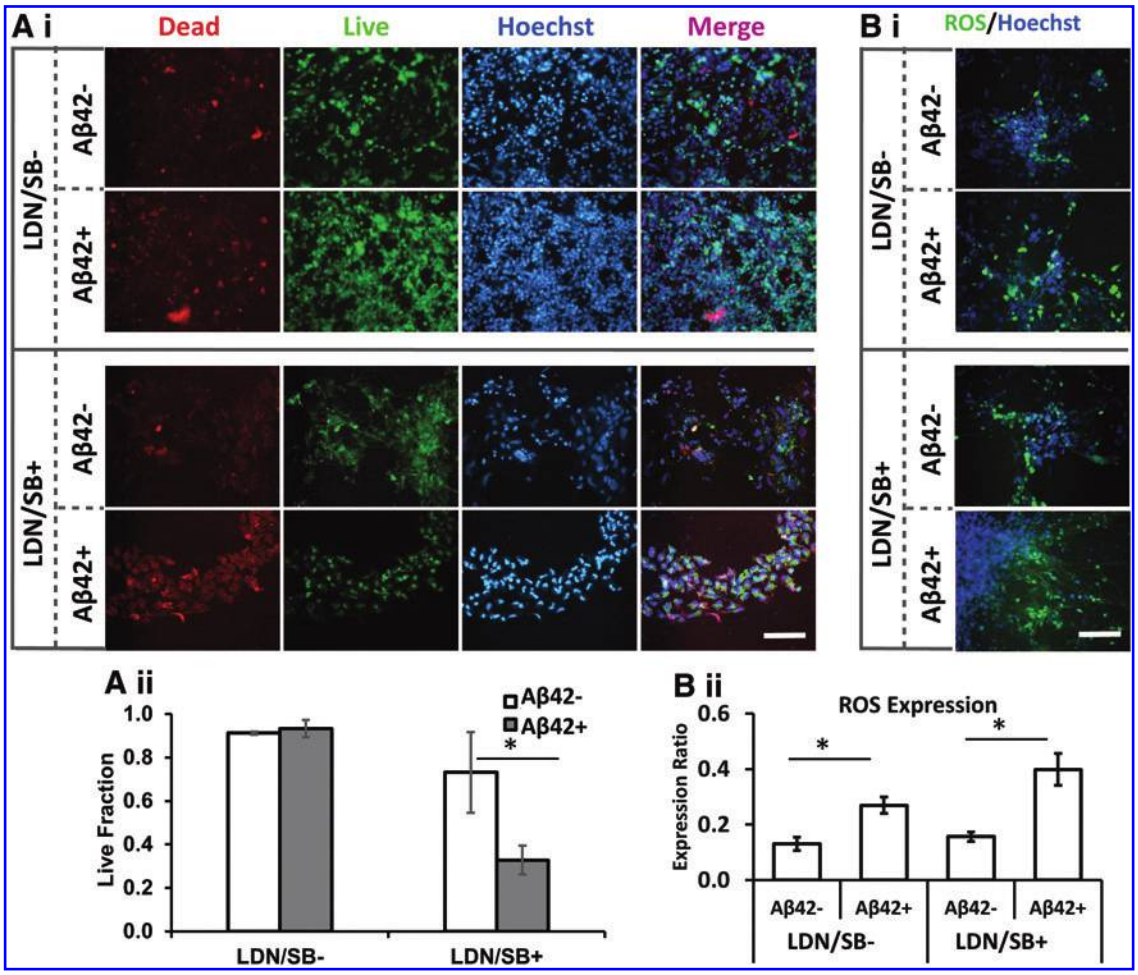

FIG. 5. Effects of Aβ42 oligomer treatment on viability and oxidative stress of iPSK3-derived asteroids. **(A)** (i) LIVE/DEAD assay images for cell viability; (ii) quantification of live cells over total cells ($n=3$). **(B)** (i) Images of ROS assay. *Blue*: Hoechst 33342 for nuclei. Scale bar: 100 μm. (ii) Quantification of ROS levels ($n=3$). *Indicates $p<0.05$. Aβ, amyloid-β; ROS, reactive oxygen species. Color images are available online.

inflammation gene expression (e.g., TNF-α and IL-6), and the transcriptome change.

Aβ42 oligomer stimulation appeared to have no significant effect on the cell viability for LDN/SB$^-$ group based on image analysis, but reduced cell viability for LDN/SB$^+$ group, probably due to the higher neuron population (Fig. 5A and Supplementary Fig. S3A). Based on two-color flow cytometry (Supplementary Fig. S3B), Aβ42 oligomer stimulation slightly increased the percentage of dead cells from 8.0% to 16.3% for the LDN/SB$^-$ group. The image analysis of ROS production suggests that Aβ42 oligomer treatment induced the oxidative stress for both of LDN/SB$^-$ and LDN/SB$^+$ groups (Fig. 5B and Supplementary Fig. S4).

VEGF-A secretion was evaluated as a proinflammatory response, since increased VEGF-A may increase the permeability of BBB and promote leukocyte extravasation.[13] In this study, Aβ42 stimulation induced VEGF-A expression for both of LDN/SB$^-$ and LDN/SB$^+$ groups (Fig. 6A). The concentration was comparable for the LDN/SB$^-$ (248 ± 18 pg/mL) and LDN/SB$^+$ cells (168 ± 69 pg/mL). RT-PCR analysis showed the upregulation of TNF-α and IL-6 with Aβ42 stimulation (3.91 ± 0.40 vs. 0.68 ± 0.47 for IL-6 and 2.90 ± 0.11 vs. 0.80 ± 0.29 for TNF-α) on LDN/SB$^-$ samples (Fig. 6Bi). These results indicate that the derived astrocyte population has proinflammation response.

RT-PCR analysis also showed the downregulation of MMP2 and MMP3, the ECM remodeling genes, with Aβ42 stimulation (0.97 ± 0.04 vs. 0.68 ± 0.04 for MMP2 and 0.85 ± 0.21 vs. 0.39 ± 0.08 for MMP3) (Fig. 6Bii). GLUT1 (glucose transporter 1) expression was slightly upregulated with Aβ42 stimulation (0.94 ± 0.09 vs. 1.20 ± 0.09) and TREM2 (Triggering receptor expressed on myeloid cells 2) was downregulated (0.97 ± 0.04 vs. 0.40 ± 0.10) (Fig. 6Biii). TREM2 in the brain may have anti-inflammatory role and interfere with the brain's ability to prevent the buildup of plaque. For example, TREM2 interacts with DAP12 in microglia to trigger phagocytosis of Aβ peptides and apoptotic neurons without inflammation.[50,51]

The effect of Aβ42 stimulation on GFAP and S100B expression was examined on LDN/SB$^-$ samples by flow cytometry (Fig. 7A). GFAP$^+$ cells decreased from 56.6% to 39.1% with Aβ42 oligomer treatment, while S100B expression remained similar (68.8% and 74.7% for −Aβ42 and +Aβ42 group, respectively). The calcium signaling in response to Aβ42 oligomer treatment was also measured (Fig. 7B). For the LDN/SB$^+$ group,

calcium signaling was more activated by ADP after Aβ42 oligomer treatment, while calcium signaling was comparable before and after Aβ42 oligomer treatment for LDN/SB^{-} group.

RNA sequencing was performed for LDN/SB^{+} cells without (minus) and with (plus) Aβ42 oligomer treatment. There were 3248 (21.8%) DEGs among a total of 14,926 detectable genes (Supplementary Fig. S5). One thousand three hundred seventeen DEGs were upregulated in the minus group and 1931 DEGs were upregulated in the plus group. A majority of astrocyte-related genes were highly expressed in the minus group (Table 1). GFAP (−0.333) and S100B (−0.474) were slightly enriched in the minus group. The gene that has the most change in fold was found to be KCNJ10 (−1.358), the potassium voltage-gated channel subfamily J member 10. The genes related to chemokines were altered between the minus and the plus groups (Table 2). CXCL9 was highly expressed in the plus group (2.275), while CCL2 (−1.565), CCL7 (−1.696), CCL3 (−1.741), CXCL1 (−1.925), and CXCL10 (−2.768) were highly expressed in the minus group. The genes related to AD were slightly changed (in the range of −0.623 to 0.703), except A2M (Table 3). A2M (−1.409) encodes alpha-2-macroglobulin, which acts as a carrier protein and binds to numerous growth factors and cytokines, such as platelet-derived growth factor, FGF-2, TGF-β, insulin, and IL-1β. For genes related to neural functions (Table 4), excitatory postsynaptic genes HOMER1 and SHANK3 had little change, but inhibitory postsynaptic gene ARHGEF9-IT1 was significantly upregulated in the plus group (2.733). Both dorsal (EMX1, SCGN, TBR1, and CALB2) and ventral (NKX2-1, DLX1, NKX2-2, and CALB1) regional markers were enriched in the minus group, as well as cortical marker FOXG1 (−1.176). The DEGs associated with brain disorders such as schizophrenia (ERG1, ERG3, and ARC) were also enriched in the minus group. Pathway analysis using Webgestalt shows that the genes in a particular pathway (e.g., Alzheimer's) were upregulated in the plus group (size = 146) (Supplementary Tables S8–S12) and the minus group (e.g., distal axon, size = 247; and synapse part, size = 809) (Supplementary Tables S13–S17) related to biological process, molecular function, cellular component, and disease.

The metabolic genes related to glycolysis and oxidative phosphorylation had little changes (from −0.316 to 0.363) (Supplementary Table S3). However, KEGG analysis shows that the plus group upregulated the genes related to oxidative phosphorylation (size = 106) (Supplementary Tables S8–S12). ECM remodeling genes MMP13 and 21 were enriched in the plus group, while MMP1, 7, 10, and 12 were enriched in the minus group (Supplementary Table S4). In addition, Wnt pathway gene WNT8A was enriched in the plus group, while WNT2 and WNT10A were enriched in the minus group (Supplementary Table S5). Moreover, MAPK pathway DUSP 2, 4, 5, and 6 genes were enriched in the minus group (Supplementary Table S6). For axon guidance genes, EFNA1

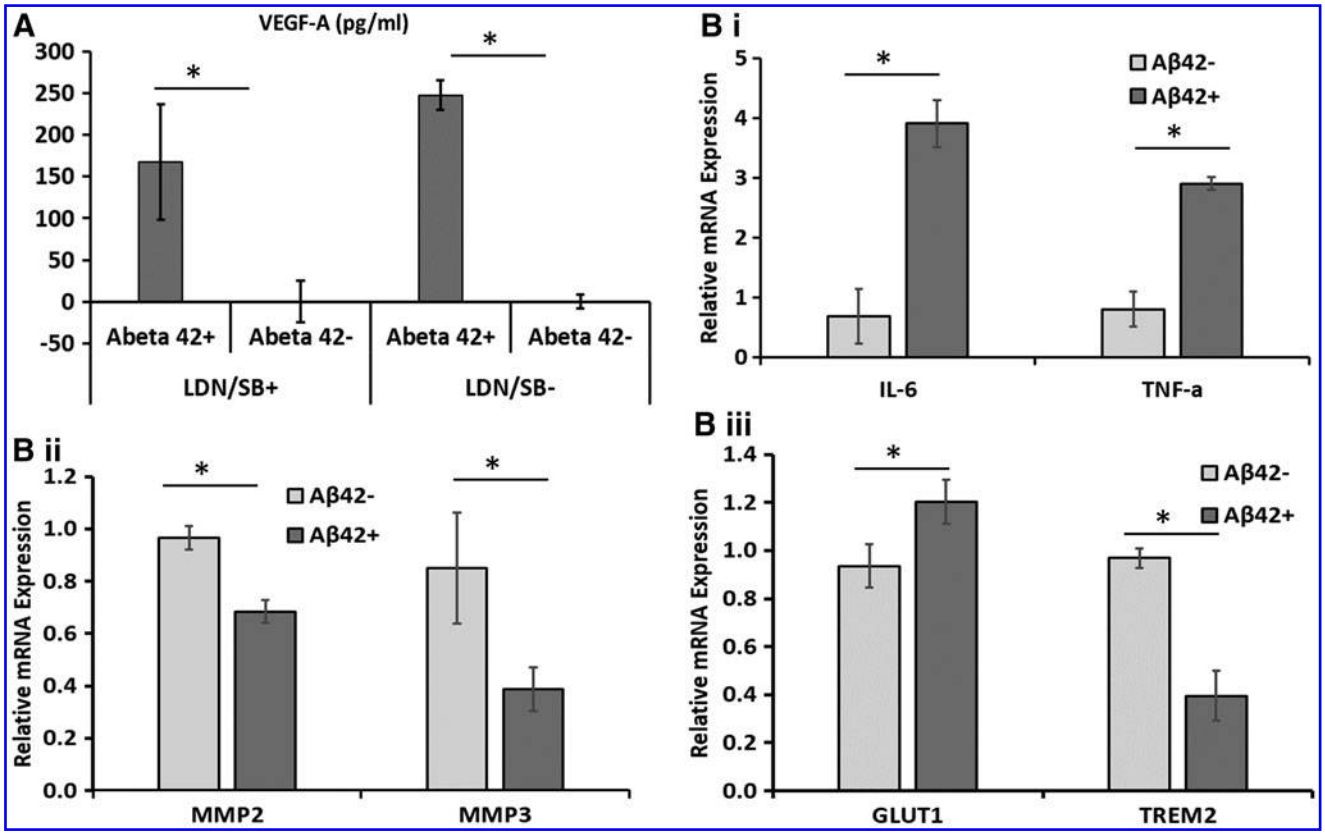

FIG. 6. Effects of Aβ42 oligomer treatment on VEGF-A secretion and gene expression of iPSK3-derived asteroids (day 50). **(A)** VEGF-A secretion of iPSK3-derived asteroids ($n = 3$). **(B)** (i) TNF-α and IL-6 gene expression by RT-PCR analysis (LDN/SB^{-} group). (ii) MMP2 and MMP3 gene expression by RT-PCR analysis (LDN/SB^{-} group). (iii) GLUT1 and TREM2 gene expression by RT-PCR analysis (LDN/SB^{-} group). $n = 3$. *Indicates $p < 0.05$. VEGF-A, vascular endothelial growth factor A.

(–1.123) and UNC5C (–0.623) were enriched in the minus group, while most of other genes had little changes (Supplementary Table S7). Taken together, Aβ42 oligomers induced transcriptome changes in the derived astrocyte-like cells.

Co-culture with cortical spheroids

Neuronal differentiation was performed using our previously published protocol (Supplementary Fig. S6).[29] The differentiated cells exhibited TBR1 (cortical layer VI), Nkx2.1 (cortical ventral cells), and β-tubulin III expression (up to 84.1%). The cells also exhibited GFAP (up to 52.2%) and tau expression. For co-culturing cortical spheroids with astrocytes, the spheroids attached onto the astrocyte layer and extensive axonal growth were observed. The culture was treated with Aβ42 oligomers, which can cause cytotoxicity of the neuronal cells (Fig. 8).[29,31,52] The cortical spheroids without co-culture showed a significant amount of dead cells (viability: 62.1% ± 5.7%), while the cortical spheroids co-cultured with astrocyte layer had higher viability (80–90%). These results indicate the neuroprotective ability of the derived astrocytes.

For co-culturing cortical spheroids with astrospheres, the astrospheres labeled with CellTracker green were observed in the cortical spheroids (Supplementary Fig. S7A). Vimentin co-staining with brain regional identity markers FOXG1, Nkx2.1, and HOXB4 indicated the cortical identity of the co-cultured spheroids and the presence of astrocytes (Supplementary Fig. S7B). The presynaptic marker synapsin I and postsynaptic marker PSD95 expression in the replated co-cultured spheroids showed the synaptic activities compared to the replated cortical spheroids alone (Supplementary Fig. S8). The quantification of synaptic activities needs electrophysiology study in the future.

Discussion

Derivation of forebrain astrocytes from iPSCs and characterizations

Our study derived the astrocytes through 3D spheroid formation, which showed >70% S100B and GFAP expression. The cells also expressed vimentin, exhibited

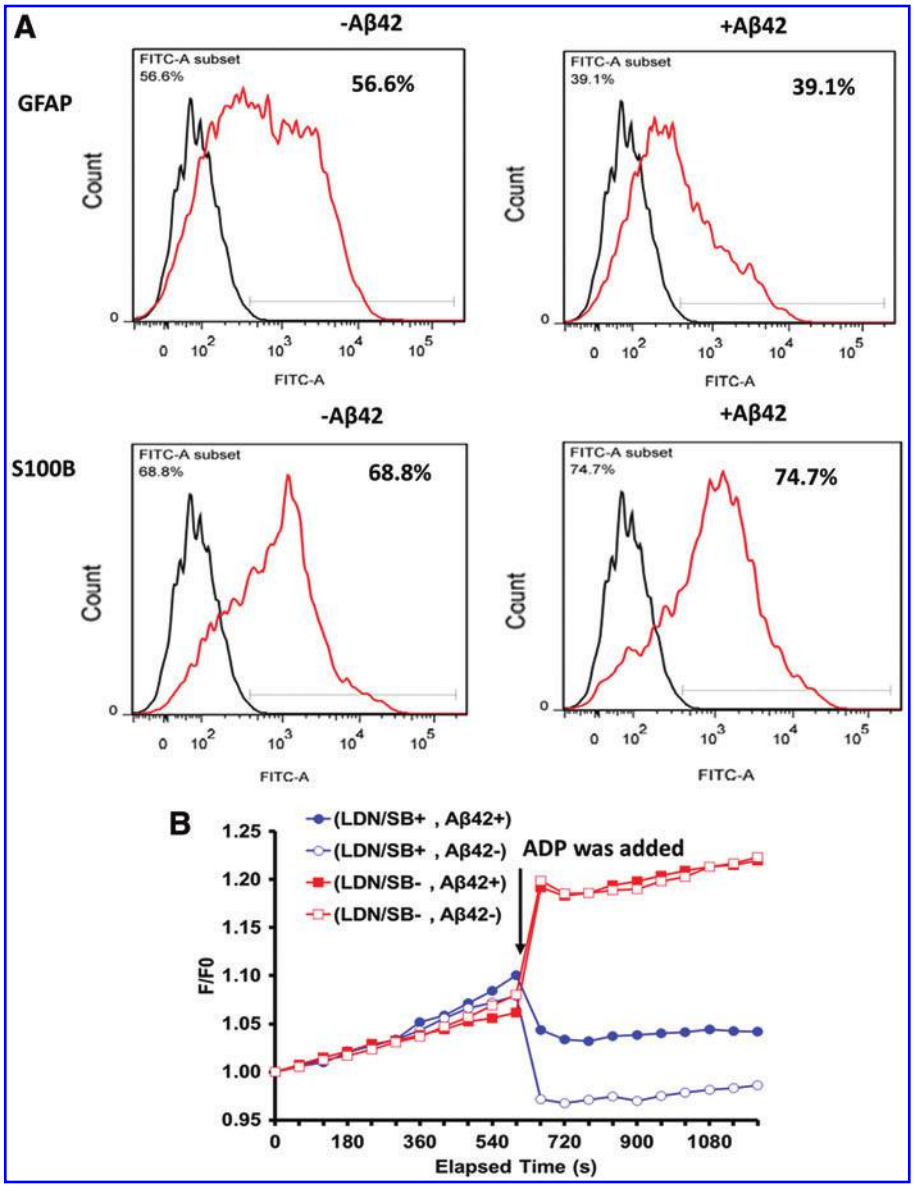

FIG. 7. Effects of Aβ42 oligomer treatment on astrocyte marker expression and calcium signaling. **(A)** Expression of GFAP and S100B determined by flow cytometry (LDN/SB$^-$ group). *Black line*: negative control; *red line*: marker of interest. **(B)** Fluorescence reading of ADP treatment-induced Ca^{2+} change from baseline, with or without Aβ42 oligomer treatment. Color images are available online.

Table 1. Genes Associated with Astrocyte-Related Phenotype

Gene name	*Base mean*	*Log2 fold change*
ALDH1L1	25.855	0.360
VIM	231888.103	0.125
GJA1	7114.245	0.024
WIF1	18.542	–0.164
NOTCH1	22238.343	–0.176
NFIA	1071.852	–0.180
SLC1A2	2282.437	–0.205
NFIB	1097.912	–0.234
HEPACAM	1.995	–0.249
SLC1A3	3391.528	–0.320
GFAP	13.492	–0.333
AQP4	51.641	–0.336
SOX9	9946.525	–0.340
TNC	523.672	–0.470
S100B	46.013	–0.474
CD44	1203.306	–0.494
NKX6-1	32.004	–0.591
NFIX	114.032	–0.977
OLIG2	156.832	–1.056
RYR3	37.329	–1.112
KCNJ10	251.734	–1.358

The numbers are the Log2 values of ratios of minus to plus. Negative values indicate that the genes are present in higher amounts in the minus group, while positive values indicate that the genes are present in higher amounts in the plus group.

Ca^{2+} signaling, and secreted CSPG and HA. Co-staining GFAP with FOXG1 (cortical dorsal identity), Nkx2.1 (cortical ventral identity), and HOXB4 (hindbrain identity), as well as RT-PCR analysis (HOXB4, NKX2.1, TBR1, NEPH3, MATH1, and OLIG2), showed that majority of cells were dorsal forebrain cortical astrocytes, although hindbrain astrocytes were also present. Astrocytes have the diversity phenotype depending on the regional neural progenitors that switch to gliogenesis.[53–55] The region-specific astrocytes may selectively support neuron growth in the corresponding region.[56] The generation of anterior hindbrain glial progenitors (which give rise to astrocytes and oligodendrocytes) expressing EN1 and GBX2 from hPSCs was recently reported.[57] Based on cerebellar differentiation in our laboratory, predominant hindbrain astrocytes may be derived by switching the cerebellar neural progenitors to gliogenesis.

Table 2. Genes Associated with Chemokines

Gene name	*Base mean*	*Log2 fold change*
CXCL9	0.492	2.275
IL16	159.440	0.223
MIF	23626.705	0.148
VEGFA	9484.308	–0.221
CCL5	1.024	–0.308
TNF	19.139	–0.402
IL17B	3.756	–0.453
IL11	145.864	–0.545
CXCL12	221.337	–0.568
CXCL16	21.137	–0.617
IL15	11.996	–1.048
CXCL2	45.320	–1.235
IL6	5.848	–1.463
CCL2	763.862	–1.565
CCL7	0.266	–1.696
CCL3	0.283	–1.741
CXCL1	23.020	–1.925
CXCL10	3.734	–2.768

The numbers are the Log2 values of ratios of minus to plus. Negative values indicate that the genes are present in higher amounts in the minus group, while positive values indicate that the genes are present in higher amounts in the plus group.

Table 3. Genes Associated to Alzheimer's Disease (Neurodegeneration)

Gene name	*Base mean*	*Log2 fold change*
CTSF	1067.602	0.703
HLA-DRB1	13.262	0.615
PLD3	17748.264	0.543
MAPT	7854.046	0.446
APP	45281.372	0.354
ABCA7	1848.781	0.256
TRIP4	946.195	0.244
SORL1	1326.684	0.225
CLU	14968.684	0.208
PSEN1	3682.795	0.165
BIN1	3191.441	0.158
PICALM	5208.351	0.106
PTK2B	427.152	0.030
PSEN2	237.199	–0.064
APOE	2053.863	–0.074
FERMT2	2490.459	–0.077
CD2AP	1547.338	–0.125
MEF2C	162.879	–0.159
CELF1	13117.991	–0.179
ZCWPW1	66.346	–0.184
CASS4	36.346	–0.187
EPHA1	13.662	–0.340
RIN3	131.679	–0.354
UNC5C	275.537	–0.623
A2M	108.303	–1.409

The numbers are the Log2 values of ratios of minus to plus. Negative values indicate that the genes are present in higher amounts in the minus group, while positive values indicate that the genes are present in higher amounts in the plus group.

The expression of both astrocyte and neuronal markers in our study indicates that the protocol results in a mixed cell population. Based on our results, the presence of LDN and SB promoted neuronal populations (43–55% vs. 15–25% β-tubulin III^+ cells, corresponding to 1:1 vs. 1:4 ratio of neurons to astrocytes, respectively). While EGF and FGF-2 are the common mitogens to maintain neural progenitors, the astrocyte induction in this study was performed using RA and heparin, which are more suitable for spheroid-based differentiation.[5,21] Other factors used previously include platelet-derived growth factor-AA[9] and fetal bovine serum.[14]

In addition, the maturation of iPSC-derived astrocytes still need further investigation in future.[19] For example, the Ca^{2+} signaling observed in this study is still preliminary. Measuring different Ca^{2+} signaling subtypes requires the maturation of iPSC-astrocytes. Moreover, the contribution of astrocytes to the synaptic activities of neurons would require electrophysiology studies. Ciliary neurotrophic factor

Table 4. Genes Related to Neural Functions and Brain Regional Markers

Gene name	*Base mean*	*Log2 fold change*
Excitatory postsynaptic		
HOMER1	666.638	–0.030
SHANK3	5991.134	0.261
Inhibitory postsynaptic		
ARHGEF9-IT1	0.669	2.733
GPHN	1555.701	0.151
Ventral		
CALB1	121.412	–0.559
NKX2-2	20.564	–0.750
DLX1	104.277	–0.949
NKX2-1	1.507	–1.190
Dorsal		
CALB2	28.325	–0.643
TBR1	196.970	–0.663
SCGN	1.023	–1.858
EMX1	1.614	–2.556
Cortical		
SATB2	278.691	0.166
PAX6	11181.644	0.009
PAX7	1514.976	–0.260
PROX1	2320.654	–0.410
FOXG1	16.606	–1.176
Ventramedial		
SLIT1	12579.859	0.406
Spinal cord		
CACNA1A	1243.881	0.158
HOXA3	4536.592	–0.029
GDF6	123.980	–0.153
HOXB4	7048.303	–0.179
HOXB3	15635.662	–0.230
KCNJ6	33.366	–0.365
Schizophrenia		
ARC	1231.107	–0.507
EGR1	7106.539	–1.097
EGR3	153.638	–1.311
Others		
GPM6A	2631.968	0.006
HSPA8	54553.583	0.071
HNRNPA1P33	8.069	0.368

The numbers are the Log2 values of ratios of minus to plus. Negative values indicate that the genes are present in higher amounts in the minus group, while positive values indicate that the genes are present in higher amounts in the plus group.

(CNTF) and bone morphogenetic protein (BMP)-4 are the common growth factors for astrocyte maturation, which can take 3 months.[2] The iPSC-astrocytes from our study may still be at the progenitor stage (40–60 days of differentiation) and the maturation may be enhanced using CNTF and BMP-4.

Immune response of iPSC-astrocytes to Aβ42 oligomers

To date, most neuroinflammatory studies on iPSC-derived astrocytes used LPS, TNF-α, and IL-1β to stimulate inflammatory response.[9,58] Different inflammation cytokines such as IL-1β, TNF-α, and IL-6 were found to differentially modulate astrocyte transcriptomes and the secretion profiles of cytokines.[58,59] However, few studies have evaluated the influence of Aβ42 oligomers. Our previous studies have used Aβ42 oligomers to evaluate the toxicity response of neuronal population only.[29,31,45] In addition, the stimulation of iPSC-derived microglia-like cells with Aβ42 oligomers was investigated for M1-type immune response.[60] In parallel, this study evaluated the stimulation of macroglia-like cells with Aβ42 oligomers, showing the increased VEGF-A secretion and upregulation of TNF-α and IL-6 by RT-PCR. The release of VEGF-A may disrupt the endothelial BBBs and increase leukocyte extravasation, therefore indicating the proinflammatory response.[13] The cell viability did not change significantly, but the oxidative stress increased. Together, our results demonstrate the proinflammation responsive properties of the derived astrocytes to Aβ42 oligomers.

Astroglia was reported to have both proinflammatory and anti-inflammatory phenotype.[13,61] Through genomics analysis, reactive astrocytes in ischemia have been shown to exhibit a molecular phenotype that is beneficial or protective for tissue repair, while reactive astrocytes induced by LPS (proinflammatory) exhibited a phenotype that may be detrimental and induce cytotoxicity.[62] Similarly, other studies also show that astrocytes can release proinflammatory molecules such as TNF-α, IL-6, VEGF, and CCLs (A1 phenotype),[13] while ischemia-caused lesion shifts astrocytes toward neuroprotective mechanism (A2 phenotype).[63,64] It was suggested that A2 phenotype might be mediated by JAK-STAT3 signaling to support neuronal regeneration, while A1-reactive astrocytes might be induced by NF-κB signaling.[63] It has been found that primary neurons co-cultured with A1 astrocytes had 50% less synapses compared to those grown with resting astrocytes.[64] Our future study needs to evaluate the A2 phenotype of the derived cells in an injury model such as ischemia stroke.

Our study also used genomics tools to evaluate the transcriptome of Aβ42 oligomer-stimulated hiPSC-astrocytes (LDN/SB^+ group) to elucidate the reactive astrocyte phenotype in response to Aβ42 oligomers. The analysis showed 21.8% of differentially expressed genes. The chemokine gene profile and brain regional marker expression (e.g., dorsal markers EMX1, SCGN, TBR1, and CALB2, and ventral markers NKX2-1, DLX1, NKX2-2, and CALB1) were altered by Aβ42 oligomers. Pathway analysis using Webgestalt showed the genes in a particular pathway (e.g., Alzheimer's) were upregulated and KEGG analysis showed that Aβ42 oligomers upregulated the genes related to oxidative phosphorylation. The immune response may be related to the exact cell population that received the treatment.

This study used healthy iPSCs for the astroglial differentiation. One step further, the disease-specific iPSCs, for example, iPSCs with PSEN1 M146V mutation used in our previous studies,[45,65] can be investigated for the differentiated macroglia plasticity and tissue homeostasis. Full recapitulation of the reactive astrocyte phenotype in the iPSC-based models is still a challenge and needs further investigated.

Astrocytes or astrosphere co-culture with isogenic cortical spheroids

Our results showed that co-culturing cortical spheroids with isogenic astrocytes has better neuroprotective ability (i.e., higher cell viability) upon Aβ42 oligomer treatment. The beneficial effects of astrocytes on neuron functions have been reported in different iPSC-based models.[21,66] For

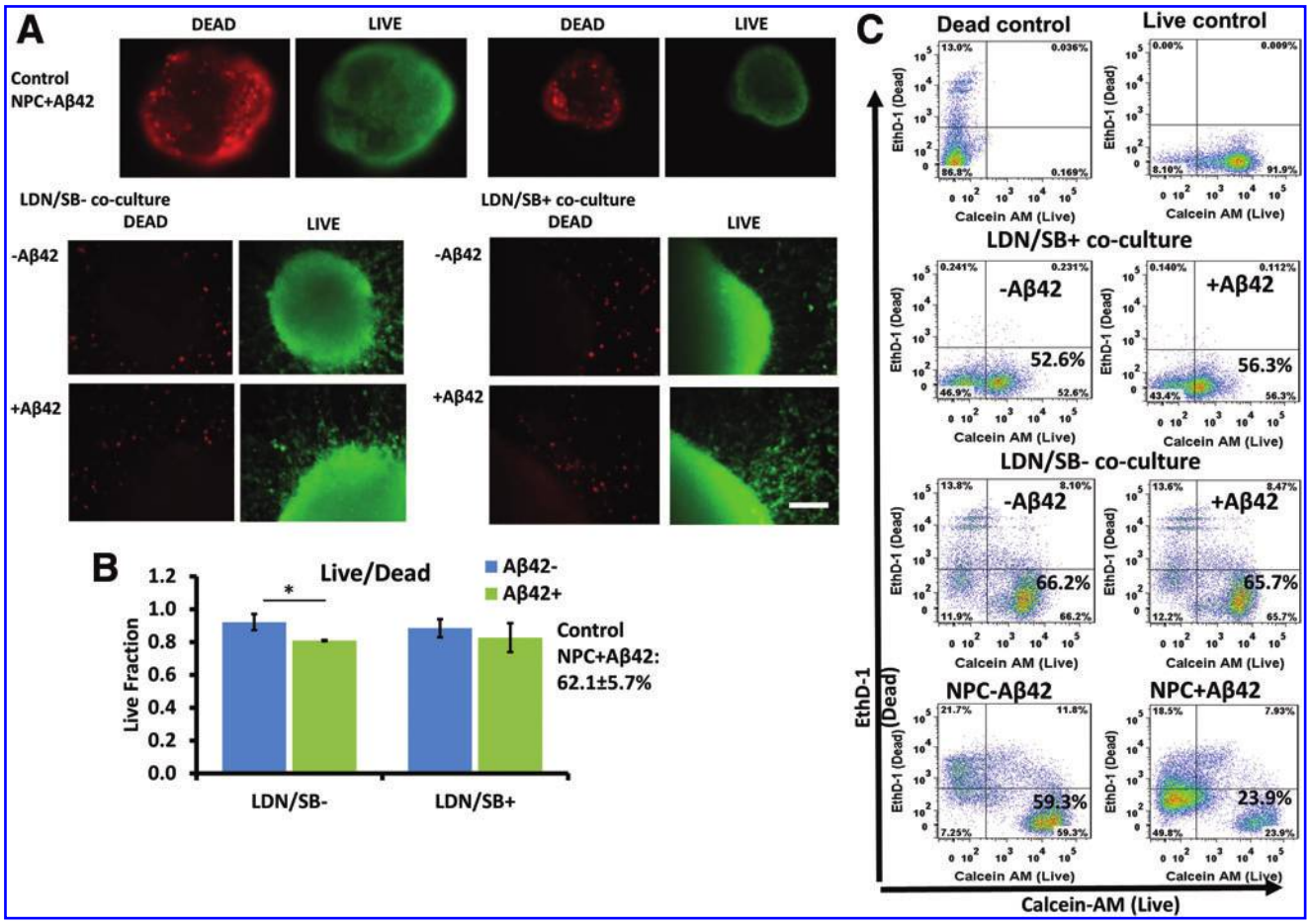

FIG. 8. Cell viability of co-cultured iPSK3 astrocytes with isogenic cortical spheroids treated with Aβ42 oligomers. Cortical spheroids (day 40) were replated onto day 53 astrocyte layer treated with Aβ42 oligomers (1 μM). LIVE/DEAD assay was performed 7 days after co-culture. **(A)** Images of LIVE/DEAD assay for the co-cultured cells. Cortical spheroids without co-culture treated with Aβ42 oligomers served as control. Scale bar: 100 μm. **(B)** Quantification of live cells over total cells ($n=3$). *Indicates $p<0.05$. **(C)** Viability of the co-cultured cortical spheroid outgrowth treated with Aβ42 oligomers (day 42) quantified by two-color flow cytometry. The cortical spheroid outgrowth was differentially harvested using Accutase. Color images are available online.

example, the hiPSC-derived neuronal models (using commercial iCells) with different ratios of excitatory and inhibitory neurons in the presence of astrocytes have been evaluated.[67] The co-cultures can be modulated with seizurogenic compounds picrotoxin and endosulfan, and the neurotoxicant methylmercury. However the chemical-induced effects on some neuronal activities, such as mean spike rate and mean burst rate, may depend on the ratio of inhibitory and excitatory neurons.[67] Co-culture of iPSC-dopaminergic neurons with astrocytes can rescue the mitochondria defects in neurons, normal neuronal differentiation, and synaptogenesis.[12] Pathogenic crosstalk between neurons and astroglial cells was also modeled based on patient-specific iPSCs, which elucidates the contribution of astrocyte-derived a-synuclein accumulation to neurodegeneration of Parkinson's disease.[68] Astrocytes also contribute to the synaptic function of the neurons,[69] indicated by electrophysiology (i.e., synaptic activities), in response to drug N-Methyl-D-aspartic acid (NMDA) and α-amino-3-hydroxy-5-methyl-4-isoxazolepropionic acid (AMPA) receptor antagonists. iPSC-astrocytes were found to promote action potential firing and synaptic activities of the iPSC-neurons.[70] It was suggested that the exosomes may be the major mediators of neuron-glia communication.[71]

iPSC-astrocytes also can be used for constructing *in vitro* BBB models. A few recent iPSC-based isogenic BBB models with three cell types (endothelial cells, neurons, and astrocytes) or including brain-specific pericytes as the fourth cell type[72] were established based on the differentiation of brain-like microvascular endothelial cells from hiPSCs.[5,6] The presence of astrocytes improved formation and maintenance of tight junctions. Our previous study assembled iPSC-derived vascular spheroids and cortical spheroids.[46] Introducing isogenic astrocytes in the 3D forebrain spheroid models may further enhance the cellular function of 3D cortical spheroids.

Conclusions

This study derived and characterized astroglial spheres from hiPSCs, which express astroglial markers and show Ca^{2+} signaling. Dual SMAD inhibition with LDN and SB enriched neuronal population. The immune response to proinflammatory factor Aβ42 oligomers was shown to alter chemokine gene profile and brain regional markers. Cell

viability did not decrease, but oxidative stress increased with Aβ42 oligomer treatment for the derived cells. The immune response also includes the increased expression of TNF-α and IL-6. Co-culturing the isogenic cortical spheroids with the derived astroglial cells showed neuroprotective ability of the co-culture. This study provides insights of reactive astrocytes as well as neural-astroglial cell interactions during neural tissue patterning from hiPSCs and has significance in 3D neural tissue modeling and degeneration/regeneration.

Acknowledgments

The authors thank Ms. Ruth Didier of FSU Department of Biomedical Sciences for her help with flow cytometry analysis, Dr. Brian K. Washburn and Kristina Poduch in FSU Department of Biological Sciences for their help with RT-PCR analysis, Dr. Cynthia Vied in FSU Translational Science Laboratory for her help in transcriptome analysis, and Dr. Stephen Duncan at Medical College of Wisconsin and Dr. David Gilbert in FSU Department of Biological Sciences for human iPSK3 cells.

Authors' Contributions

K.G. did all the differentiation experiments and most characterizations. J.B. and L.S. helped characterizations and data analysis. M.M. helped some characterizations. T.H. and Q.S. helped the differentiation of Ep-iPSC line and RT-PCR analysis. R.J. helped data analysis and article review. Y.L. conceived the projects, and wrote and revised the article.

Disclosure Statement

No competing financial interests exist.

Funding Information

This work is supported by FSU Bridge Grant and NSF CAREER Award (No. 1652992 to Y.L.).

Supplementary Material

Supplementary Data
Supplementary Figure S1
Supplementary Figure S2
Supplementary Figure S3
Supplementary Figure S4
Supplementary Figure S5
Supplementary Figure S6
Supplementary Figure S7
Supplementary Figure S8
Supplementary Table S1
Supplementary Table S2
Supplementary Table S3
Supplementary Table S4
Supplementary Table S5
Supplementary Table S6
Supplementary Table S7
Supplementary Table S8
Supplementary Table S9
Supplementary Table S10
Supplementary Table S11
Supplementary Table S12
Supplementary Table S13
Supplementary Table S14
Supplementary Table S15
Supplementary Table S16
Supplementary Table S17

References

1. Tao, Y., and Zhang, S.C. Neural subtype specification from human pluripotent stem cells. Cell Stem Cell **19,** 573, 2016.
2. Oksanen, M., Petersen, A.J., Naumenko, N., *et al.* PSEN1 mutant iPSC-derived model reveals severe astrocyte pathology in Alzheimer's disease. Stem Cell Reports **9,** 1885, 2017.
3. Olsen, M.L., Khakh, B.S., Skatchkov, S.N., Zhou, M., Lee, C.J., and Rouach, N. New insights on astrocyte ion channels: critical for homeostasis and neuron-glia signaling. J Neurosci **35,** 13827, 2015.
4. Appelt-Menzel, A., Cubukova, A., Gunther, K., *et al.* Establishment of a human blood-brain barrier co-culture model mimicking the neurovascular unit using induced pluri- and multipotent stem cells. Stem Cell Rep **8,** 894, 2017.
5. Canfield, S.G., Stebbins, M.J., Morales, B.S., *et al.* An isogenic blood-brain barrier model comprising brain endothelial cells, astrocytes, and neurons derived from human induced pluripotent stem cells. J Neurochem **140,** 874, 2017.
6. Patel, R., Page, S., and Al-Ahmad, A.J. Isogenic blood-brain barrier models based on patient-derived stem cells display inter-individual differences in cell maturation and functionality. J Neurochem **142,** 74, 2017.
7. Zhang, Y., Sloan, S.A., Clarke, L.E., *et al.* Purification and characterization of progenitor and mature human astrocytes reveals transcriptional and functional differences with mouse. Neuron **89,** 37, 2016.
8. Dowell, J.A., Johnson, J.A., and Li, L. Identification of astrocyte secreted proteins with a combination of shotgun proteomics and bioinformatics. J Proteome Res **8,** 4135, 2009.
9. Santos, R., Vadodaria, K.C., Jaeger, B.N., *et al.* Differentiation of inflammation-responsive astrocytes from glial progenitors generated from human induced pluripotent stem cells. Stem Cell Rep **8,** 1757, 2017.
10. Khakh, B.S., and Sofroniew, M.V. Diversity of astrocyte functions and phenotypes in neural circuits. Nat Neurosci **18,** 942, 2015.
11. Dezonne, R.S., Sartore, R.C., Nascimento, J.M., *et al.* Derivation of functional human astrocytes from cerebral organoids. Sci Rep **7,** 45091, 2017.
12. Du, F., Yu, Q., Chen, A., Chen, D., and Yan, S.S. Astrocytes attenuate mitochondrial dysfunctions in human dopaminergic neurons derived from iPSC. Stem Cell Rep **10,** 366, 2018.
13. Sofroniew, M.V. Astrocyte barriers to neurotoxic inflammation. Nat Rev Neurosci **16,** 249, 2015.
14. Tcw, J., Wang, M., Pimenova, A.A., *et al.* An efficient platform for astrocyte differentiation from human induced pluripotent stem cells. Stem Cell Rep **9,** 600, 2017.
15. Canals, I., Ginisty, A., Quist, E., *et al.* Rapid and efficient induction of functional astrocytes from human pluripotent stem cells. Nat Methods **15,** 693, 2018.
16. Li, X., Tao, Y., Bradley, R., *et al.* Fast generation of functional subtype astrocytes from human pluripotent stem cells. Stem Cell Rep **11,** 998, 2018.

17. Lischka, F.W., Efthymiou, A., Zhou, Q., *et al.* Neonatal mouse cortical but not isogenic human astrocyte feeder layers enhance the functional maturation of induced pluripotent stem cell-derived neurons in culture. Glia **66,** 725, 2018.
18. Bradley, R.A., Shireman, J., McFalls, C., *et al.* Regionally specified human pluripotent stem cell-derived astrocytes exhibit different molecular signatures and functional properties. Development **146,** 2019. pii: dev170910.
19. Sloan, S.A., Darmanis, S., Huber, N., *et al.* Human astrocyte maturation captured in 3D cerebral cortical spheroids derived from pluripotent stem cells. Neuron **95,** 779, 2017.
20. Pasca, A.M., Sloan, S.A., Clarke, L.E., *et al.* Functional cortical neurons and astrocytes from human pluripotent stem cells in 3D culture. Nat Methods **12,** 671, 2015.
21. Krencik, R., Seo, K., van Asperen, J.V., *et al.* Systematic three-dimensional coculture rapidly recapitulates interactions between human neurons and astrocytes. Stem Cell Rep **9,** 1745, 2017.
22. Zhao, J., Davis, M.D., Martens, Y.A., *et al.* APOE epsilon4/epsilon4 diminishes neurotrophic function of human iPSC-derived astrocytes. Hum Mol Genet **26,** 2690, 2017.
23. Lin, Y.T., Seo, J., Gao, F., *et al.* APOE4 Causes Widespread molecular and cellular alterations associated with Alzheimer's disease phenotypes in human iPSC-derived brain cell types. Neuron **98,** 1141, 2018.
24. Si-Tayeb, K., Noto, F.K., Sepac, A., *et al.* Generation of human induced pluripotent stem cells by simple transient transfection of plasmid DNA encoding reprogramming factors. BMC Dev Biol **10,** 81, 2010.
25. Si-Tayeb, K., Noto, F.K., Nagaoka, M., *et al.* Highly efficient generation of human hepatocyte-like cells from induced pluripotent stem cells. Hepatology **51,** 297, 2010.
26. Yan, Y., Martin, L., Bosco, D., *et al.* Differential effects of acellular embryonic matrices on pluripotent stem cell expansion and neural differentiation. Biomaterials **73,** 231, 2015.
27. Bejoy, J., Song, L., Zhou, Y., and Li, Y. Wnt-Yes associated protein interactions during neural tissue patterning of human induced pluripotent stem cells. Tissue Eng Part A **24,** 546, 2018.
28. Song, L., Wang, K., Li, Y., and Yang, Y. Nanotopography promoted neuronal differentiation of human induced pluripotent stem cells. Colloids Surf B: Biointerfaces **148,** 49, 2016.
29. Yan, Y., Bejoy, J., Xia, J., Guan, J., Zhou, Y., and Li, Y. Neural patterning of human induced pluripotent stem cells in 3-D cultures for studying biomolecule-directed differential cellular responses. Acta Biomater **42,** 114, 2016.
30. Yan, Y., Song, L., Madinya, J., Ma, T., and Li, Y. Derivation of cortical spheroids from human induced pluripotent stem cells in a suspension bioreactor. Tissue Eng Part A **24,** 418, 2018.
31. Bejoy, J., Song, L., Wang, Z., Sang, Q.X., Zhou, Y., and Li, Y. Neuroprotective activities of heparin, heparinase III, and hyaluronic acid on the Aβ42-treated forebrain spheroids derived from human stem cells. ACS Biomater Sci Eng **4,** 2922, 2018.
32. Sart, S., Yan, Y., Li, Y., *et al.* Crosslinking of extracellular matrix scaffolds derived from pluripotent stem cell aggregates modulates neural differentiation. Acta Biomater **30,** 222, 2016.
33. Sart, S., Ma, T., and Li, Y. Extracellular matrices decellularized from embryonic stem cells maintained their structure and signaling specificity. Tissue Eng Part A **20,** 54, 2014.
34. Sart, S., Calixto Bejarano, F., Baird, M.A., *et al.* Intracellular labeling of mouse embryonic stem cell-derived neural progenitor aggregates with micron-sized particles of iron oxide. Cytotherapy **17,** 98, 2015.
35. Yan, Y., Calixto Bejarano, F., Sart, S., *et al.* Cryopreservation of embryonic stem cell-derived multicellular neural aggregates labeled with micron-sized particles of iron oxide for magnetic resonance imaging. Biotechnol Prog **31,** 510, 2015.
36. Sart, S., Ma, T., and Li, Y. Cryopreservation of pluripotent stem cell aggregates in defined protein-free formulation. Biotechnol Prog **29,** 143, 2013.
37. Sart, S., Yan, Y., and Li, Y. The microenvironment of embryoid bodies modulated the commitment to neural lineage post-cryopreservation. Tissue Eng Part C Methods **21,** 356, 2015.
38. Vied, C., Ray, S., Badger, C.D., Bundy, J.L., Arbeitman, M.N., and Nowakowski, R.S. Transcriptomic analysis of the hippocampus from six inbred strains of mice suggests a basis for sex-specific susceptibility and severity of neurological disorders. J Comp Neurol **524,** 2696, 2016.
39. Dobin, A., Davis, C.A., Schlesinger, F., *et al.* STAR: ultrafast universal RNA-seq aligner. Bioinformatics **29,** 15, 2013.
40. Love, M.I., Huber, W., and Anders, S. Moderated estimation of fold change and dispersion for RNA-seq data with DESeq2. Genome Biol **15,** 550, 2014.
41. Wang, J., Duncan, D., Shi, Z., and Zhang, B. WEB-based GEne SeT AnaLysis Toolkit (WebGestalt): update 2013. Nucleic Acids Res **41,** (Web Server issue), W77, 2013.
42. Zhang, B., Kirov, S., and Snoddy, J. WebGestalt: an integrated system for exploring gene sets in various biological contexts. Nucleic Acids Res **33,** (Web Server issue), W741, 2005.
43. Benjamini, Y., and Hochberg, Y. Controlling the false discovery rate: a practical and powerful approach to multiple testing. J R Stat Soc Ser B **57,** 289, 1995.
44. Bejoy, J., Wang, Z., Bijonowski, B., *et al.* Differential effects of heparin and hyaluronic acid on neural patterning of human induced pluripotent stem cells. ACS Biomater Sci Eng **4,** 4354, 2018.
45. Yan, Y., Song, L., Bejoy, J., *et al.* Modelling neurodegenerative microenvironment using cortical organoids derived from human stem cells. Tissue Eng Part A **24,** 1125, 2018.
46. Song, L., Yuan, X., Jones, Z., *et al.* Assembly of human stem cell-derived cortical spheroids and vascular spheroids to model 3-D brain-like tissues. Sci Rep **9,** 5977, 2019.
47. Muguruma, K., Nishiyama, A., Kawakami, H., Hashimoto, K., and Sasai, Y. Self-organization of polarized cerebellar tissue in 3D culture of human pluripotent stem cells. Cell Rep **10,** 537, 2015.
48. Khakh, B.S., and McCarthy, K.D. Astrocyte calcium signaling: from observations to functions and the challenges therein. Cold Spring Harb Perspect Biol **7,** a020404, 2015.
49. Hu, N.W., Corbett, G.T., Moore, S., *et al.* Extracellular forms of Abeta and Tau from iPSC models of Alzheimer's disease disrupt synaptic plasticity. Cell Rep **23,** 1932, 2018.
50. Zheng, H., Jia, L., Liu, C.C., *et al.* TREM2 promotes microglial survival by activating Wnt/beta-catenin pathway. J Neurosci **37,** 1772, 2017.
51. Zhong, L., Wang, Z., Wang, D., *et al.* Amyloid-beta modulates microglial responses by binding to the triggering

receptor expressed on myeloid cells 2 (TREM2). Mol Neurodegener **13,** 15, 2018.
52. Vazin, T., Ball, K.A., Lu, H., *et al.* Efficient derivation of cortical glutamatergic neurons from human pluripotent stem cells: a model system to study neurotoxicity in Alzheimer's disease. Neurobiol Dis **62,** 62, 2014.
53. Krencik, R., Weick, J.P., Liu, Y., Zhang, Z.-J., and Zhang, S.-C. Specification of transplantable astroglial subtypes from human pluripotent stem cells. Nat Biotechnol **29,** 528, 2011.
54. Krencik, R., and Zhang, S.-C. Directed differentiation of functional astroglial subtypes from human pluripotent stem cells. Nat Protoc **6,** 1710, 2011.
55. Ebert, A.D., Shelley, B.C., Hurley, A.M., *et al.* EZ spheres: a stable and expandable culture system for the generation of pre-rosette multipotent stem cells from human ESCs and iPSCs. Stem Cell Res **10,** 417, 2013.
56. Morel, L., Chiang, M.S.R., Higashimori, H., *et al.* Molecular and functional properties of regional astrocytes in the adult brain. J Neurosci **37,** 8706, 2017.
57. Yun, W., Hong, W., Son, D., *et al.* Generation of anterior hindbrain-specific, glial-restricted progenitor-like cells from human pluripotent stem cells. Stem Cells Dev **28,** 633, 2019.
58. Zhou, Q., Viollet, C., Efthymiou, A., *et al.* Neuroinflammatory astrocytes generated from cord blood-derived human induced pluripotent stem cells. J Neuroinflammation **16,** 164, 2019.
59. Perriot, S., Mathias, A., Perriard, G., *et al.* Human induced pluripotent stem cell-derived astrocytes are differentially activated by multiple sclerosis-associated cytokines. Stem Cell Rep **11,** 1199, 2018.
60. Song, L., Yuan, X., Jones, Z., *et al.* Functionalization of brain region-specific spheroids with isogenic microglia-like cells. Sci Rep **9,** 11055, 2019.
61. Almad, A., and Maragakis, N.J. A stocked toolbox for understanding the role of astrocytes in disease. Nat Rev Neurol **14,** 351, 2018.
62. Zamanian, J.L., Xu, L., Foo, L.C., *et al.* Genomic analysis of reactive astrogliosis. J Neurosci **32,** 6391, 2012.
63. Liddelow, S.A., and Barres, B.A. Reactive astrocytes: production, function, and therapeutic potential. Immunity **46,** 957, 2017.
64. Liddelow, S.A., Guttenplan, K.A., Clarke, L.E., *et al.* Neurotoxic reactive astrocytes are induced by activated microglia. Nature **541,** 481, 2017.
65. Marzano, M., Bejoy, J., Cheerathodi, M., *et al.* Differential effects of extracellular vesicles of lineage-specific human pluripotent stem cells on cellular behaviours of isogenic cortical spheroids. Cells **8,** 993, 2019.
66. Russo, F.B., Freitas, B.C., Pignatari, G.C., *et al.* Modeling the interplay between neurons and astrocytes in autism using human induced pluripotent stem cells. Biol Psychiatry **83,** 569, 2018.
67. Tukker, A.M., Wijnolts, F.M.J., de Groot, A., and Westerink, R.H.S. Human iPSC-derived neuronal models for in vitro neurotoxicity assessment. Neurotoxicology **67,** 215, 2018.
68. di Domenico, A., Carola, G., Calatayud, C., *et al.* Patient-specific iPSC-derived astrocytes contribute to non-cell-autonomous neurodegeneration in Parkinson's disease. Stem Cell Rep **12,** 213, 2019.
69. Krencik, R., van Asperen, J.V., and Ullian, E.M. Human astrocytes are distinct contributors to the complexity of synaptic function. Brain Res Bull **129,** 66, 2017.
70. Ishii, M.N., Yamamoto, K., Shoji, M., Asami, A., and Kawamata, Y. Human induced pluripotent stem cell (hiPSC)-derived neurons respond to convulsant drugs when co-cultured with hiPSC-derived astrocytes. Toxicology **389,** 130, 2017.
71. Fruhbeis, C., Frohlich, D., Kuo, W.P., and Kramer-Albers, E.M. Extracellular vesicles as mediators of neuron-glia communication. Front Cell Neurosci **7,** 182, 2013.
72. Canfield, S.G., Stebbins, M.J., Faubion, M.G., Gastfriend, B.D., Palecek, S.P., and Shusta, E.V. An isogenic neurovascular unit model comprised of human induced pluripotent stem cell-derived brain microvascular endothelial cells, pericytes, astrocytes, and neurons. Fluids Barriers CNS **16,** 25, 2019.

Address correspondence to:
Yan Li, PhD
Department of Chemical and Biomedical Engineering
FAMU-FSU College of Engineering
Florida State University
2525 Pottsdamer Street
Tallahassee, FL 32310
USA

E-mail: yli4@fsu.edu

Received: August 20, 2019
Accepted: November 5, 2019
Online Publication Date: December 11, 2019